Cosmic microwave background bispectrum from the lensing-Rees-Sciama correlation reexamined: Effects of nonlinear matter clustering

Veronika Junk and Eiichiro Komatsu

Phys. Rev. D **85**, 123524 — Published 15 June 2012

DOI: 10.1103/PhysRevD.85.123524

Cosmic Microwave Background Bispectrum from the Lensing–Rees-Sciama Correlation Reexamined: Effects of Non-linear Matter Clustering

Veronika Junk
University Observatory Munich, Scheinerstr. 1, D-81679 Munich, Germany

Eiichiro Komatsu
Texas Cosmology Center and the Department of Astronomy, The University of Texas at Austin, 1 University Station, C1400, Austin, TX 78712
Kavli Institute for the Physics and Mathematics of the Universe, Todai Institutes for Advanced Study, the University of Tokyo, Kashiwa, Japan 277-8583 (Kavli IPMU, WPI) and
Max Planck Institut für Astrophysik, Karl-Schwarzschild-Str. 1, 85741 Garching, Germany

The bispectrum of the cosmic microwave background (CMB) generated by a correlation between a time-dependent gravitational potential and the weak gravitational lensing effect provides a direct measurement of the influence of dark energy on CMB. This bispectrum is also known to yield the most important contamination of the so-called "local-form" primordial bispectrum, which can be used to rule out all single-field inflation models. In this paper, we reexamine the effect of non-linear matter clustering on this bispectrum. We compare three different approaches: the 3rd-order perturbation theory (3PT), and two empirical fitting formulae available in the literature, finding that detailed modeling of non-linearity appears to be not very important, as most of the signal-to-noise comes from the squeezed triangle, for which the correlation in the linear regime dominates. The expected signal-to-noise ratio for an experiment dominated by the cosmic variance up to $l_{\rm max} = 1500$ is about 5, which is much smaller than the previous estimates including non-linearity, but agrees with the estimates based on the linear calculation. We find that the difference between the linear and non-linear predictions is undetectable, and does not alter the contamination of the local-form primordial non-Gaussianity.

I. INTRODUCTION

A time-dependent gravitational potential changes the temperature of the cosmic microwave background (CMB) as $\delta T/T = 2\int dt\ (\partial\Psi/\partial t)$ [1, 2], where Ψ is a perturbation to the time-time component of the Friedmann-Lemaître-Robertson-Walker metric. As Ψ is constant during the matter-dominated era, a detection of this effect directly shows that the universe is not completely matter-dominated, but has contributions from either spatial curvature or dark energy. Given the tight constraint on the spatial curvature we have from the current cosmological data [3], a detection of this effect is considered as the direct evidence for the effect of dark energy on the growth of structure [4].

The weak gravitational lensing effect caused by matter density fluctuations between us and the last scattering surface also changes the temperature of CMB, by shifting the observed directions of photons as $T(\hat{\mathbf{n}}) \to T(\hat{\mathbf{n}}+\mathbf{d}) = T(\hat{\mathbf{n}}) + \mathbf{d}\cdot\nabla T(\hat{\mathbf{n}}) + \ldots$ [5]. Here, the deflection angle $\mathbf{d}$ is given by $\mathbf{d} = 2\int dr \frac{r_*-r}{r r_*}\nabla\Psi(\hat{\mathbf{n}}r)$. As the same Ψ enters in both effects, these two effects are correlated, yielding a non-zero 3-point correlation (bispectrum) in the CMB [6]. Therefore, this bispectrum can be used to probe the nature of dark energy [7].

The time-dependence of Ψ is caused by two effects: one is the linear growth, and the other is the *non-linear* growth. The former effect is caused by dark energy slowing down the growth of structure, leading to a decay of Ψ. The latter effect is caused by non-linear evolution of density fluctuations, leading to a growth of Ψ. Following the literature, we shall call the former the "integrated Sachs–Wolfe (ISW; [1]) effect," and the latter the "Rees–Sciama (RS; [2]) effect." In this paper, we shall calculate the bispectrum generated by the lensing-ISW correlation on large scales as well as the lensing-RS correlation on small scales.

The main focus of this paper is the lensing-RS correlation. This correlation has been studied in the past [7–9] with different empirical methods for computing the non-linear matter power spectrum. In this paper, we systematically compare two empirical methods used in the literature and the 3rd-order perturbation theory (3PT), which is applied to the lensing-RS bispectrum for the first time in this paper. We find that, while these different methods yield somewhat different results for the lensing-RS bispectrum, the differences are too small to detect or affect our interpretation of the data.

In Sec. II, we review the lensing-RS bispectrum. In Sec. III, we compare three methods for computing the non-linear matter power spectrum. In Sec. IV, we compare the lensing-RS cross-correlation power spectrum, $Q(l)$, computed with different non-linear matter power spectra. In Sec. V, we calculate the expected signal-to-noise ratio of the lensing-RS bispectrum and the χ^2 differences between the linear model and various non-linear models. In Sec. VI, we study the effects of non-linearity on the contamination of the local-form primordial non-Gaussianity parameter, $f_{\rm NL}$. We conclude in Sec VII.

Throughout this paper, we shall use the cosmologi-

cal parameters given by the WMAP 5-year best-fit parameters (WMAP+BAO+H_0 ML; [10]): $\Omega_M = 0.277$, $\Omega_\Lambda = 0.723$, $h = 0.702$, $n_s = 0.962$, and $\sigma_8 = 0.817$.

II. LENSING-RS BISPECTRUM

Let us use spherical harmonics to expand the observed temperature anisotropy, $\delta T(\hat{\mathbf{n}})/T = \sum a_{lm} Y_{lm}(\hat{\mathbf{n}})$, as well as the "lensing potential," $\Theta(\hat{\mathbf{n}}) = \sum_{lm} \Theta_{lm} Y_{lm}(\hat{\mathbf{n}})$, defined by $\mathbf{d} \equiv \nabla\Theta$. Then, the CMB bispectrum generated by the lensing-RS correlation is given by [6, 11]

$$B^{m_1m_2m_3}_{l_1l_2l_3} \equiv \langle a_{l_1m_1} a_{l_2m_2} a_{l_3m_3} \rangle = \mathcal{G}^{m_1m_2m_3}_{l_1l_2l_3} \left[\frac{l_1(l_1+1) - l_2(l_2+1) + l_3(l_3+1)}{2} \times C^P_{l_1} \langle \Theta^*_{l_3m_3} a^{\rm ISW}_{l_3m_3} \rangle + 5\, perm. \right]. \quad (1)$$

Here, C^P_l is the primary CMB power spectrum without lensing, and $a^{\rm ISW}_{lm}$ are the spherical harmonics coefficients of the ISW (or RS) effect.

However, Eq. (1) is the leading-order contribution which is accurate only to $\sim 10\%$ level at $l \gtrsim 2000$. Lewis, Challinor and Hanson [12] have shown that the sub-leading-order correction can be incorporated by simply replacing C^P_l above with the *lensed* CMB power spectrum, C_l:

$$B^{m_1m_2m_3}_{l_1l_2l_3} = \mathcal{G}^{m_1m_2m_3}_{l_1l_2l_3} \left[\frac{l_1(l_1+1) - l_2(l_2+1) + l_3(l_3+1)}{2} \times C_{l_1} \langle \Theta^*_{l_3m_3} a^{\rm ISW}_{l_3m_3} \rangle + 5\, perm. \right]. \quad (2)$$

We shall use this formula for computing the lensing-ISW (RS) bispectrum. Note that this prescription of replacing C^P_l with C_l is accurate only for the bispectrum in the squeezed configuration where one of the wavenumbers, say, l_1, is much smaller than the other two, i.e., $l_1 \ll l_2 \approx l_3$. This is sufficient for our purpose because the signal-to-noise ratio of the lensing-ISW (or RS) bispectrum is dominated by the squeezed configuration.

The Gaunt integral, $\mathcal{G}^{m_1m_2m_3}_{l_1l_2l_3}$, is defined as

$$\mathcal{G}^{m_1m_2m_3}_{l_1l_2l_3} \equiv \sqrt{\frac{(2l_1+1)(2l_2+1)(2l_3+1)}{4\pi}} \times \begin{pmatrix} l_1 & l_2 & l_3 \\ 0 & 0 & 0 \end{pmatrix} \begin{pmatrix} l_1 & l_2 & l_3 \\ m_1 & m_2 & m_3 \end{pmatrix}. \quad (3)$$

Assuming statistical isotropy of the universe, rotational invariance implies that one can average over orientation of triangles (i.e., m's) to obtain the angle-averaged bispectrum [13]:

$$B_{l_1l_2l_3} \equiv \sum_{m_1m_2m_3} \begin{pmatrix} l_1 & l_2 & l_3 \\ m_1 & m_2 & m_3 \end{pmatrix} B^{m_1m_2m_3}_{l_1l_2l_3} = \sqrt{\frac{(2l_1+1)(2l_2+1)(2l_3+1)}{4\pi}} \begin{pmatrix} l_1 & l_2 & l_3 \\ 0 & 0 & 0 \end{pmatrix} \times \left[\frac{l_1(l_1+1) - l_2(l_2+1) + l_3(l_3+1)}{2} \times C_{l_1} \langle \Theta^*_{l_3m_3} a^{\rm ISW}_{l_3m_3} \rangle + 5\, perm. \right]. \quad (4)$$

Here, the cross-power spectrum of the lensing potential and the ISW (or RS) effect, $Q(l) \equiv \langle \Theta^*_{l_3m_3} a^{\rm ISW}_{l_3m_3} \rangle$, is given by [6, 7]

$$Q(l) \equiv \langle \Theta^*_{l_3m_3} a^{\rm ISW}_{l_3m_3} \rangle = 2 \int_0^{z_*} dz \frac{r(z_*) - r(z)}{r(z_*) r(z)^3} \left. \frac{\partial P_\Psi(k,z)}{\partial z} \right|_{k=l/r(z)}, \quad (5)$$

where $z_* = 1090$ is the redshift of the last scattering surface, P_Ψ the power spectrum of the Newtonian potential:

$$P_\Psi(k,z) = \left(\frac{3}{2} \Omega_M \right)^2 \left(\frac{H_0}{k} \right)^4 P(k,z) (1+z)^2, \quad (6)$$

and $P(k)$ the power spectrum of matter density fluctuations, δ_M. This result follows from the Poisson equation (in natural units): $k^2\Psi(k,z) = -4\pi G \rho_M(z) a^2(z) \delta_M(k,z) = -4\pi G \rho_{M0} \delta_M(k,z)(1+z) = -\frac{3}{2}\Omega_M H_0^2 \delta_M(k,z)(1+z)$.

On large scales where the scale-invariant spectrum, $P_\Psi \propto 1/k^3$, is still preserved, the cross-power spectrum goes as $Q(l) \propto 1/l^3$. On the other hand, the primary power spectrum goes as $C^{\rm P}_l \propto 1/l^2$. On smaller scales, $Q(l)$ falls even faster than $1/l^3$. This implies that the bispectrum peaks at the "squeezed triangle," for which one of l's is much smaller than the other two (e.g., $l_3 \ll l_1 \simeq l_2$ if we order multipoles such that $l_3 \le l_2 \le l_1$), and the smallest l corresponds to l of $Q(l)$. This observation suggests that the signal would be dominated by $Q(l)$ in the small l for which matter fluctuations can still be treated as linear perturbations, and thus the detailed modeling of non-linear fluctuations may not be necessary. We will confirm this observation in this paper.

The remaining task is to calculate $P(k,z)$, including non-linear matter clustering.

III. NONLINEAR MATTER POWER SPECTRUM

A. 3rd-order Perturbation Theory (3PT)

Higher-order perturbation theory is a promising approach for computing non-linear evolution of matter density fluctuations [14]. This is especially true at high redshifts ($z > 1$), where non-linearity is not too strong [15]. The lensing-RS correlation has been studied using the 3rd-order perturbation theory (3PT) by [16], who found a reasonable agreement between the 3PT prediction and the data obtained from the N-body simulation.[1]

[1] Due to a page limitation, Ref. [16] did not report on the details of the 3PT results in the published version; however, the details are reported in arXiv:0711.1696.

The matter power spectrum including the next-to-leading order non-linear correction is given by [17]

$$P(k,z) = [D(z)]^2 P_{11}(k) + [D(z)]^4 [2P_{13}(k) + P_{22}(k)], \quad (7)$$

where $D(z)$ is a suitably normalized linear growth factor (which is proportional to the scale factor during the matter era), $P_{11}(k)$ is the linear power spectrum at an arbitrary initial time, z_i, at which $D(z_i)$ is normalized to unity, and $P_{22}(k)$ and $P_{13}(k)$ are given by

$$P_{22}(k) = 2\int \frac{d^3q}{(2\pi)^3} P_{11}(q) P_{11}(|\mathbf{k}-\mathbf{q}|) \left[F_2^{(s)}(\mathbf{q}, \mathbf{k}-\mathbf{q})\right]^2, \quad (8)$$

where

$$F_2^{(s)}(\mathbf{k}_1, \mathbf{k}_2) = \frac{5}{7} + \frac{2}{7}\frac{(\mathbf{k}_1\cdot\mathbf{k}_2)^2}{k_1^2 k_2^2} + \frac{\mathbf{k}_1\cdot\mathbf{k}_2}{2}\left(\frac{1}{k_1^2} + \frac{1}{k_2^2}\right), \quad (9)$$

and

$$\begin{aligned} 2P_{13}(k) = {} & \frac{2\pi k^2}{252} P_{11}(k) \int_0^\infty \frac{dq}{(2\pi)^3} P_{11}(q) \\ & \times \left[100\frac{q^2}{k^2} - 158 + 12\frac{k^2}{q^2} - 42\frac{q^4}{k^4} \right. \\ & \left. + \frac{3}{k^5 q^3}(q^2-k^2)^3(2k^2+7q^2)\ln\left(\frac{k+q}{|k-q|}\right)\right] \end{aligned} \quad (10)$$

The 3PT is an attractive approach, as it provides the *exact* calculation in the quasi linear regime where the perturbative expansion is still valid. This should be contrasted with the empirical approaches described below: they are calibrated using numerical simulations with a specific set of cosmological parameters, and thus cannot be easily extended to other cosmological models, such as dynamical dark energy models.

A disadvantage of the 3PT is that its validity is limited to the quasi linear regime, and thus the result on very small scales cannot be trusted. One can check the validity of the 3PT calculation by comparing it to a direct numerical simulation [15, 16]; or, one can compare an empirical formula calibrated to a specific cosmological model, to the 3PT calculation using the same cosmological model. We shall adopt the latter approach in this paper.

B. Empirical Models

Empirical approaches, which are calibrated using N-body simulations, have an advantage that they can, in principle, describe the matter power spectrum in a highly non-linear regime where the perturbative expansion breaks down. We shall use one of the popular methods, called the "halo model," [18] for checking the validity of the 3PT for computing the lensing-RS power spectrum. We then compare these results with another empirical model [19] used by most of the previous work on the lensing-RS bispectrum.

1. Halo Model (HALOFIT)

In the halo model, the matter power spectrum is decomposed into two pieces: one that arises from two-point correlations between dark matter particles residing in two different dark matter halos (2-halo term), and another that arises from two-point correlations between dark matter particles residing in a single dark matter halo (1-halo term). The former contribution is given approximately by the linear matter power spectrum, whereas the latter contribution is given by the density profile of dark matter halos. This splitting between the 2- and 1-halo terms is somewhat artificial, and thus the halo model approach would not provide an accurate description of the non-linear matter power spectrum, unless it is calibrated by numerical simulations.

One popular calibrated formula is due to Smith et al. [20], which will be called "HALOFIT." They model the power spectrum as $P(k) = P_Q(k) + P_H(k)$, where $P_Q(k)$ is the quasi-linear 2-halo term:

$$P_Q(k) = P_{11}(k)\frac{\left[1 + k^3 P_{11}(k)/(2\pi^2)\right]^{\beta_n}}{1 + \alpha_n k^3 P_{11}(k)/(2\pi^2)} \exp\left[-f(y)\right], \quad (11)$$

where $f(y) \equiv y/4 + y^2/8$ with $y = k/k_\sigma$, and α_n, β_n, and k_σ are free parameters which need to be determined from simulations (see Appendix C of [20]). The second term, $P_H(k)$, is the 1-halo term:

$$P_H(k) = \frac{1}{1 + \mu_n/y + \nu_n/y^2} \frac{a_n y^{3f_1}}{1 + b_n y^{f_2} + [c_n f_3 y]^{3-\gamma_n}}, \quad (12)$$

where μ_n, ν_n, a_n, b_n, c_n, γ_n, f_1, f_2, and f_3 are free parameters which need to be determined from simulations. As one of the cosmological models for which these functions are calibrated is a ΛCDM model with $\Omega_M = 0.3$, $\Omega_\Lambda = 0.7$, $h = 0.7$, and $\sigma_8 = 0.9$, which is close to the parameters we adopt in this paper, this model can be used to check the validity of the 3PT results in the non-linear regime. However, we remind the readers that HALOFIT is not guaranteed to provide accurate results for the cosmological models that are not explored in Ref. [20], such as dynamical dark energy or massive neutrino models. Ref. [9] also used HALOFIT for computing the lensing-RS bispectrum.

2. HKLM Scaling Model (MA99)

Another empirical formula is based on the idea originally put forward by HKLM [21] for the real-space two-point correlation function. This idea has been applied to the power spectrum by [22, 23]. Then, Ma et al. [19] have extended the calibration to include models with dynamical dark energy. We shall use the formula of Ma et al., and call it "MA99."

HKLM postulates that the non-linear correlation function is a universal function of the linear correlation

function, once the length scale (or the wavenumber) is rescaled by the mass conservation (i.e., transformation from Lagrangian to Eulerian coordinates). The form of this universal function needs to be found from numerical simulations. Ma et al. [19] find

$$\frac{k^3P(k,z)}{2\pi^2} = G\left[\frac{k_0^3P_{11}(k_0,z)/(2\pi^2)}{g_0^{3/2}[\sigma_8(z)]^\beta}\right]\frac{k_0^3P_{11}(k_0,z)}{2\pi^2}, \tag{13}$$

where $\beta = 0.83$, $\sigma_8(z)$ is related to the present-day σ_8 by $\sigma_8(z) = [D(z)/D(0)]\sigma_8$, and g_0 is defined by $g_0 \equiv |w|^{1.3|w|-0.76}g(0)$. Here, $g(z) \propto (1+z)D(z)$, but it is normalized such that $g(z_i) = 1$ during the matter-dominated era (e.g., $z_i = 30$).[2] The Lagrangian wavenumber, k_0, is related to the Eulerian wavenumber, k, as

$$k_0 \equiv \frac{k}{[1 + k^3P(k,z)/(2\pi^2)]^{1/3}}. \tag{14}$$

The function, $G(x)$, is given by

$$G(x) = [1 + \ln(1 + 0.5x)]\,\frac{1 + 0.02x^4 + c_1x^8/g(z)^3}{1 + c_2x^{7.5}}, \tag{15}$$

with $c_1 = 1.08 \times 10^{-4}$ and $c_2 = 2.10 \times 10^{-5}$.

How do we compute $P(k,z)$ using this formula?[3]

1. Compute the linear power spectrum, $P_{11}(k_0,z)$, for a given Lagrangian wavenumber, k_0.
2. Compute $G(x)$ in Eq. (13), and multiply it by $k_0^3P_{11}(k_0,z)/(2\pi^2)$ to obtain $k^3P(k,z)/(2\pi^2)$.
3. Compute the Eulerian wavenumber, k, using Eq. (14).
4. Compute $P(k,z)$ from $k^3P(k,z)/(2\pi^2)$ times $(2\pi^2)/k^3$.

C. Comparing $P(k,z)$

In Figure 1, we show non-linear power spectra at $z = 0.1$ and 1 computed from 3PT (solid line), MA99 (dotted line), and HALOFIT (dashed line). We find that, somewhat surprisingly, HALOFIT and Ma et al. for $z = 0.1$ are fairly discrepant at $k \approx 0.3 - 3\ h\ \mathrm{Mpc}^{-1}$. (MA99 underestimates the power relative to HALOFIT.)

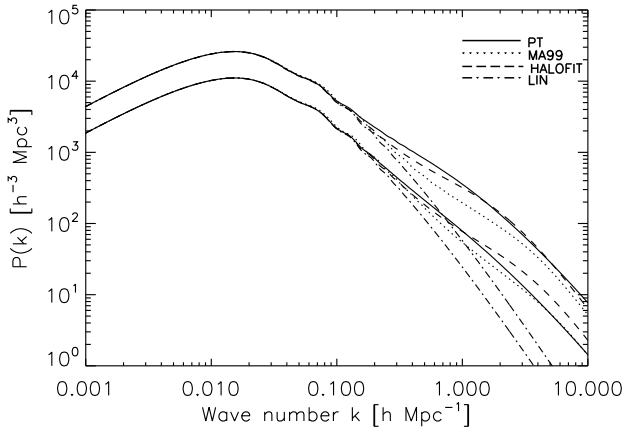

FIG. 1. Comparison of non-linear power spectra computed from 3PT (solid line), MA99 (dotted line), and HALOFIT (dashed line). The linear power spectrum is shown by the dashed-dotted line. The upper and lower curves show $P(k,z)$ for $z = 0.1$ and 1, respectively.

In order to identify the origin of this discrepancy, we have also compared MA99 and HALOFIT with the formula by Peacock and Dodds (1996; PD96) [23] (not shown in Figure 1; in order to use their formula, it is necessary to use the smooth linear power spectrum without baryonic oscillations; thus, we used the smooth power spectrum given in [24]). We find that PD96 and HALOFIT agree well, which is consistent with the finding of [9]. However, MA99 and PD96, which are based on the same HKLM idea, differ significantly. This probably indicates that the difference already existed at the level of N-body simulations used by MA99 and PD96. Given that the latest HALOFIT formula has been shown to provide excellent fits to a wide range of N-body simulations, we conclude that PD96 and HALOFIT are more accurate than MA99. This suggests that the previous work based on MA99 [7, 8] would require a reexamination.

On the other hand, the 3PT results are close to HALOFIT, but lie slightly above it at $k \approx 0.2 - 1\ h\ \mathrm{Mpc}^{-1}$. This is a known result: at a low redshift, the 3PT tends to overpredict the non-linear power spectrum [15]. While this is an issue for the 1%-level precision cosmology using the galaxy power spectrum, the discrepancy at this level may not be so bad for the calculation of the lensing-RS correlation, as the statistical error on the expected total signal-to-noise of the measurement of the lensing-RS bispectrum is modest ($S/N \lesssim 10$). We thus take this as an encouraging sign and move on.

[2] For example, $g(0) = 0.7646$ for $\Omega_M = 0.277$, $\Omega_\Lambda = 0.723$ and $w = -1$.

[3] While this formula has been used by most of the previous work on the lensing-RS bispectrum [7, 8], in all cases it has been implemented incorrectly. In the previous work, the authors used Eq. (13) with k_0 in the argument of $G(x)$ replaced by k. This is not the implementation proposed by the original paper [19], and goes against the original proposal made by HKLM. This observation gave an initial motivation for our work.

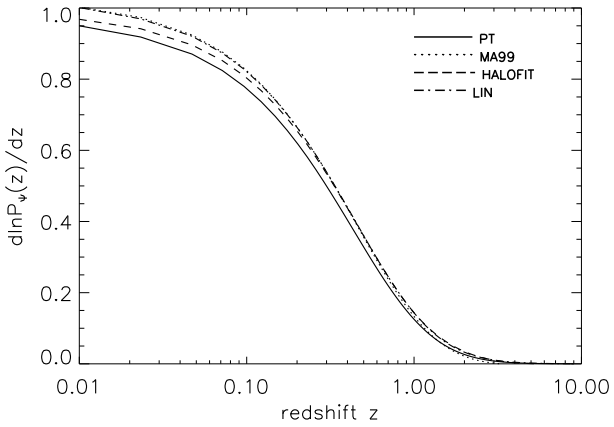

FIG. 2. Comparison of $\partial \ln P_\Psi(k,z)/\partial z$ for $k = 0.1\ h\,\mathrm{Mpc}^{-1}$ as a function of z, computed from 3PT (solid line), MA99 (dotted line), and HALOFIT (dashed line).

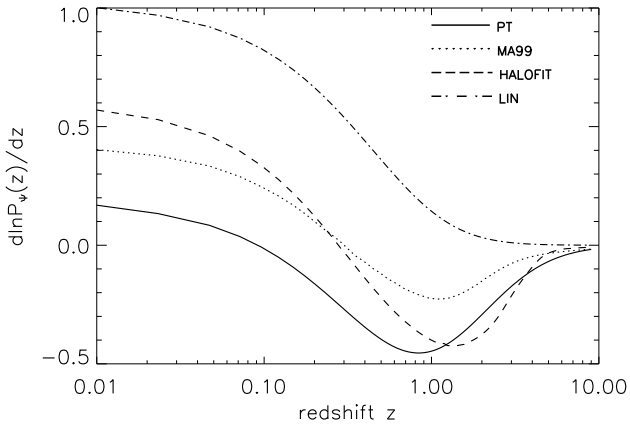

FIG. 3. Same as Figure 2, but for $k = 1\ h\,\mathrm{Mpc}^{-1}$.

IV. LENSING-RS CROSS-POWER SPECTRUM

A. $\partial \ln P_\Psi(k,z)/\partial z$

The essential ingredient of the lensing-RS bispectrum is the lensing-RS cross-power spectrum, $Q(l)$, defined by Eq. (5). In order to compute $Q(l)$, we need derivatives of the potential power spectrum, P_Ψ, with respect to redshifts, $\partial P_\Psi(k,z)/\partial z$. This is related to derivatives of the density power spectrum, $P(k,z)$, as (see Eq. (6))

$$\frac{\partial \ln P_\Psi(k,z)}{\partial z} = \frac{\partial \ln P(k,z)}{\partial z} + \frac{2}{(1+z)}. \qquad (16)$$

As $P(k,z) \propto (1+z)^{-2}$ for the linear matter power spectrum during the matter-dominated era, $\partial P_\Psi(k,z)/\partial z$ vanishes for this case, as expected. When the universe is dominated by curvature or dark energy, the first term is still negative but becomes smaller than the second term, yielding $\partial P_\Psi(k,z)/\partial z > 0$. On the other hand, the 3PT result (Eq. (7)) shows that non-linear evolution gives a term in $P(k,z)$ which goes as $(1+z)^{-4}$, and thus one obtains non-zero $\partial P_\Psi(k,z)/\partial z$ even during the matter-dominated era. The sign is opposite: $\partial P_\Psi(k,z)/\partial z < 0$.

We find that one needs to be quite careful about numerical accuracy when computing $\partial \ln P_\Psi(k,z)/\partial z$. A stable result can be obtained by the following method: compute $\ln P_\Psi(k,z)$ for various redshifts separated by $\delta z = 10^{-2}$, and then use a cubic spline interpolation to evaluate the derivative. For $y(z) \equiv \ln P_\Psi(k,z)$,

$$y'(z) = \frac{y(z_{\rm hi}) - y(z_{\rm low})}{z_{\rm hi} - z_{\rm low}} + \frac{1}{6}[(3B^2-1)y''(z_{\rm hi}) - (3A^2-1)y''(z_{\rm low})](z_{\rm hi} - z_{\rm low}), \qquad (17)$$

where $A \equiv (z_{\rm hi} - z)/(z_{\rm hi} - z_{\rm low})$ and $B \equiv (z - z_{\rm low})/(z_{\rm hi} - z_{\rm low})$, and $z_{\rm hi}$ and $z_{\rm low}$ denote the pre-computed values of redshifts that are closest to the chosen value of z. See Sec. 3.3 of [25]. This method gives a highly accurate $\partial P_\Psi(k,z)/\partial z$ compared to a simpler numerical differentiation such as $y(z) = [y(z+\delta z/2) - y(z-\delta z/2)]/\delta z$ or $y(z) = [y(z+\delta z) - y(z)]/\delta z$. We have verified this using the 3PT results: for 3PT, one can calculate the derivative exactly by differentiating Eq. (7) with respect to z:

$$\frac{\partial P(k,z)}{\partial z} = 2D(z)\frac{dD}{dz}\left\{P_{11}(k) + 2[D(z)]^2\left[2P_{13}(k) + P_{22}(k)\right]\right\}. \qquad (18)$$

We find that the derivative from Eq. (18) and that from the cubic spline interpolation agree precisely.[4]

In Figure 2, we show $\partial \ln P_\Psi(k,z)/\partial z$ for $k = 0.1\ h\,\mathrm{Mpc}^{-1}$ as a function of z, computed from 3PT (solid line), MA99 (dotted line), HALOFIT (dashed line), and the linear spectrum (dot-dashed line). At this wavenumber, they roughly agree with each other to within 5% at $z \geq 0.01$. Non-linear evolution of matter fluctuations makes $\partial \ln P_\Psi(k,z)/\partial z$ slightly smaller than the linear prediction. At this wavenumber, the predicted non-linearity is the largest for 3PT, followed by HALOFIT and MA99, which is consistent with Figure 1.

In Figure 3, we show $\partial \ln P_\Psi(k,z)/\partial z$ for $k = 1\ h\ \mathrm{Mpc}^{-1}$. This regime is quite non-linear, and thus we see a clear change in the sign of $\partial \ln P_\Psi(k,z)/\partial z$ at a moderate redshift. (Recall that the linear evolution due to dark energy gives a positive contribution to

[4] We suspect that any differences between our results presented in this paper and those presented in the literature [7–9] can be explained by either an incorrect implementation of MA99 or an inaccurate computation of the derivative or both. A code for reproducing our results is available on http://www.mpa-garching.mpg.de/~komatsu/CRL/

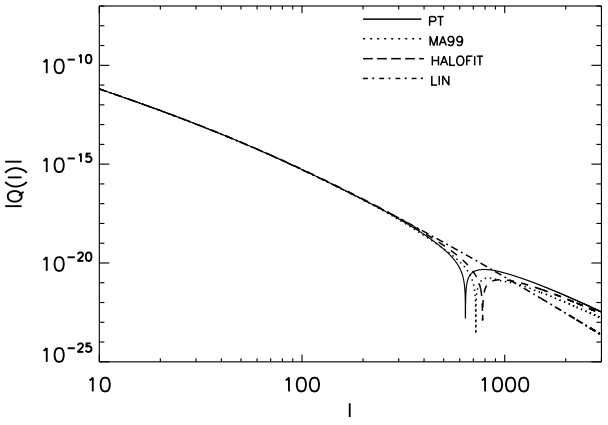

FIG. 4. Absolute values of the lensing-RS cross-power spectrum, $|Q(l)|$, as a function of multipoles, l, computed from 3PT (solid line), MA99 (dotted line), and HALOFIT (dashed line). The linear power spectrum result, which does not show any change of the sign, is shown by the dashed-dotted line. Note that the sign of $Q(l)$ is positive on large angular scales and negative on small angular scales.

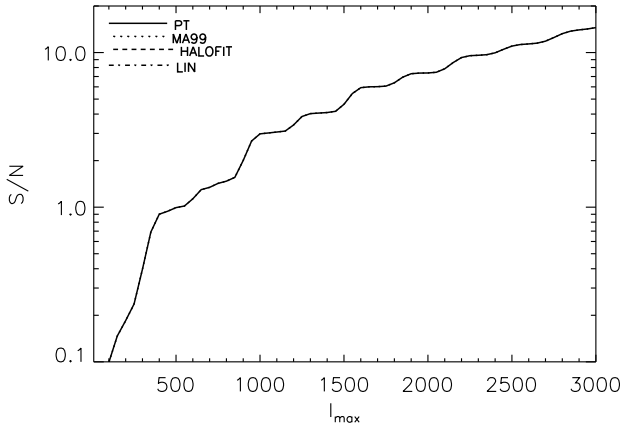

FIG. 5. Expected signal-to-noise ratio of the lensing-RS bispectrum, S/N, as a function of the maximum multipole, $l_{\rm max}$. All non-linear models as well as the linear model give similar results.

$\partial \ln P_\Psi(k,z)/\partial z$, while the non-linear evolution gives a negative contribution to $\partial \ln P_\Psi(k,z)/\partial z$.) The precise redshift at which the sign changes depends on models of non-linearity: it is $z \sim 0.1$ for 3PT while it is $z \sim 0.3$ for HALOFIT and MA99.

B. $Q(l)$

With $\partial P_\Psi/\partial z$ computed, we now compute the lensing-RS power spectrum, $Q(l)$, from Eq. (5). In Figure 4, we show $|Q(l)|$ computed from 3PT (solid line), MA99 (dotted line) and HALOFIT (dashed line). The sign change due to non-linearity is seen, and the multipole at which the sign changes depends on models of non-linearity. It is $l \sim 640$, 700, and 800 for 3PT, MA99, and HALOFIT, respectively.

V. RESULTS

A. Signal-to-noise ratio

How well can we measure the lensing-RS bispectrum? The expected signal-to-noise ratio is given by [13]

$$\left(\frac{S}{N}\right)^2 \equiv \frac{1}{6}\sum_{2\le l_1 l_2 l_3 \le l_{\rm max}} \frac{B^2_{l_1 l_2 l_3}}{C_{l_1}C_{l_2}C_{l_3}} = \sum_{2\le l_1\le l_2\le l_3 < l_{\rm max}} \frac{B^2_{l_1 l_2 l_3}}{\Delta_{l_1 l_2 l_3} C_{l_1}C_{l_2}C_{l_3}}, \quad (19)$$

where $\Delta_{l_1 l_2 l_3} = 1$ if all l's are different, $\Delta_{l_1 l_2 l_3} = 2$ if two l's are equal (isosceles configuration), and $\Delta_{l_1 l_2 l_3} = 6$ if all l's are equal (equilateral configuration).

This formula assumes that non-Gaussianity is weak, and the covariance matrix of the bispectrum can be approximated by the Gaussian piece, $C_{l_1}C_{l_2}C_{l_3}$. However, Lewis, Challinor and Hanson have shown that there is a non-negligible contribution from the non-Gaussian signal generated by the lensing-ISW bispectrum to the covariance matrix [12]. We shall ignore this contribution for simplicity, as our primary goal here is to investigate how non-linear RS effect changes the signal-to-noise ratio relative to the linear ISW effect. As a result, our signal-to-noise ratio is overestimated by 10% at $l_{\rm max} = 1500$ and by $\gtrsim 40\%$ at $l_{\rm max} \gtrsim 2000$. As all the previous work except for [12] has also ignored this contribution to the covariance matrix, our results for the signal-to-noise ratio can be compared directly with those from the previous work.

In Figure 5, we show S/N as a function of the maximum multipole, $l_{\rm max}$. We find that all non-linear models as well as the linear model give similar results. This confirms our earlier observation (see Sec. II) that the lensing-RS bispectrum peaks in the squeezed limit where the smallest multipole corresponds to l of $Q(l)$, and thus most of the signal-to-noise comes from the region where $Q(l)$ is well approximated by the linear lensing-ISW cross-correlation power spectrum. Our S/N estimate agrees well with that from the linear calculation of [26].

Note that our S/N for the linear model is about a factor of 2.7 smaller than that of [9].[5] Their Eq. (15) suggests that they have not restricted the sum to $l_1 \le$

[5] For this comparison, we use Eq. (1) instead of Eq. (2) because

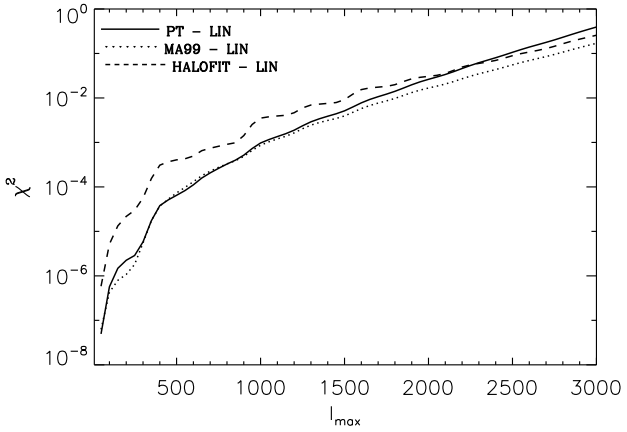

FIG. 6. The χ^2 differences between the linear model and various non-linear models: 3PT (solid line), MA99 (dotted line), and HALOFIT (dashed line).

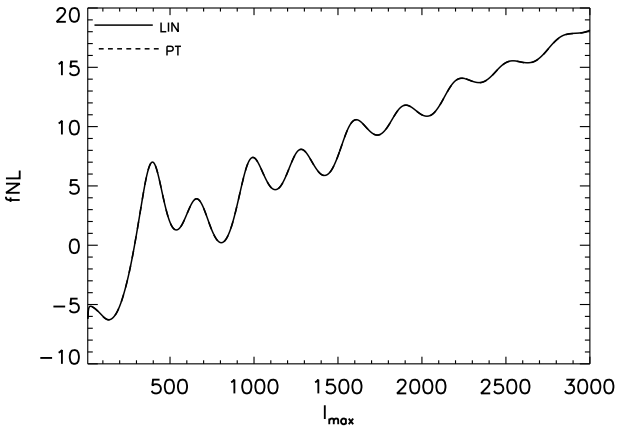

FIG. 7. The contamination of $f_{\rm NL}$ due to the lensing-ISW (linear effect only; solid line) and the lensing-RS (3PT; dashed line). Non-linearity does not affect the contamination of $f_{\rm NL}$. The solid and dashed lines are indistinguishable.

$l_2 \leq l_3$, which results in an overestimation of $(S/N)^2$ by a factor of 6, i.e., a factor 2.4 in S/N, which is enough to explain the difference.

Our S/N for the non-linear model using MA99 is an order of magnitude smaller than that of [8].[5] This is probably due to a combination of their not restricting the sum to $l_1 \leq l_2 \leq l_3$ and their overestimating the bispectrum with an incorrect implementation of MA99 (see Sec. III B 2).

B. χ^2 difference between linear and non-linear models

Can we detect differences between the linear and non-linear models? In order to answer this question, we calculate the χ^2 differences between the linear and non-linear models from [9]

$$\chi^2_{\rm X-Y} \equiv \sum_{2\leq l_1\leq l_2\leq l_3<l_{\rm max}} \frac{\left(B^{\rm X}_{l_1l_2l_3} - B^{\rm Y}_{l_1l_2l_3}\right)^2}{\Delta_{l_1l_2l_3} C_{l_1} C_{l_2} C_{l_3}}, \qquad (20)$$

where X and Y denote the names of models under consideration. For example, when we study the χ^2 difference between 3PT and the linear model, $X =$ 3PT and $Y =$ LIN.

In Figure 6, we show the χ^2 differences between the linear model and various non-linear models: $\chi^2_{X-\rm LIN}$ for $X =$ 3PT, MA99, and HALOFIT. We find that, for all non-linear models, the χ^2 differences are much smaller than unity, indicating that the differences are too small to detect. We find similar values of χ^2 differences among non-linear models.

Our results do not agree with those of [9], who find $\chi^2_{X-\rm LIN}$ of order unity for $X =$ HALOFIT. We suspect that this is potentially due to (i) their not restricting the sum to $l_1 \leq l_2 \leq l_3$ (which would account for a factor of 6), and (ii) a numerical accuracy of their evaluation of $\partial P_\Psi(k,z)/\partial z$. As noted in Sec. IV A, a simple derivative such as $\partial P_\Psi(k,z)/\partial z = [P_\Psi(k, z+\delta z) - P_\Psi(k,z)]/\delta z$ can result in an inaccurate result, and a better method such as the cubic spline interpolation is needed for correctly calculating this derivative. We have confirmed this by using the above simple derivative, finding that the results can vary significantly if such simpler numerical derivatives are used.

VI. CONTAMINATION OF THE LOCAL-FORM PRIMORDIAL NON-GAUSSIANITY

While the lensing-ISW and lensing-RS bispectra are useful for studying the nature of dark energy, they are also important because they yield the largest known contamination of the so-called "local form" primordial bispectrum [26–28]. The local-form bispectrum is particularly important, as a significant detection of the *primordial* bispectrum of this form would rule out all single-field inflation models regardless of the details of models [29].

The contamination of the local-form primordial bispectrum, parametrized by the $f_{\rm NL}$ parameter, has been computed for the lensing-ISW bispectrum. How would non-linearity (lensing-RS) affect $f_{\rm NL}$? To answer this question, we calculate the "bias in $f_{\rm NL}$," i.e., a value of $f_{\rm NL}$ which would be found if we fit the lensing-RS bispec-

they have used the unlensed C_l when calculating the lensing-RS bispectrum.

trum to the local-form primordial bispectrum template:

$$\delta f_{\rm NL} = \frac{\sum_{l_1\le l_2\le l_3} \frac{B^{\rm prim}_{l_1l_2l_3} B^{\rm lens-RS}_{l_1l_2l_3}}{\Delta_{l_1l_2l_3} C_{l_1} C_{l_2} C_{l_3}}}{\sum_{l_1\le l_2\le l_3} \frac{(B^{\rm prim}_{l_1l_2l_3})^2}{\Delta_{l_1l_2l_3} C_{l_1} C_{l_2} C_{l_3}}}, \qquad (21)$$

where $B^{\rm prim}_{l_1l_2l_3}$ is the local-form primordial bispectrum given in [11].

In Figure 7, we show the contamination of $f_{\rm NL}$ for the lensing-ISW (solid) and the lensing-RS (computed with 3PT; dashed) bispectra. We find that they give similar results, and thus non-linearity does not affect the contamination of $f_{\rm NL}$. The values of $\delta f_{\rm NL}(l_{\rm max})$ that we find agree well with those from the linear calculation of [28].

VII. CONCLUSIONS

The basic findings of this paper are simple: while non-linear matter clustering modifies the shape of the lensing-ISW bispectrum, differences between the linear prediction and non-linear predictions as well as differences among non-linear predictions are too small to detect. Non-linearity does not affect the contamination of the local-form primordial bispectrum. This is because the lensing-ISW bispectrum peaks in the squeezed configuration in which the smallest multipole corresponds to the multipole of the lensing-ISW cross-correlation power spectrum, where the linear approximation is valid. Therefore, the linear calculation would be practically sufficient when interpreting the CMB data such as those from Planck.

Nevertheless, if one wishes to improve upon the linear calculation, one should probably use the 3PT, as it offers a greater flexibility in terms of cosmological models for which the calculations are valid, as well as a straightforward computation of $\partial P_\Psi(k,z)/\partial z$.

Our results do not agree with the previous work studying the lensing-RS bispectrum [7–9] which found much greater effects of non-linear clustering on the lensing-RS bispectrum. We suspect that the discrepancy is due to a combination of an incorrect implementation of MA99, an inaccurate numerical evaluation of $\partial P_\Psi(k,z)/\partial z$, and/or their not restricting the sum in $(S/N)^2$ to $l_1 \le l_2 \le l_3$. As a result, the expected signal-to-noise ratio of the lensing-RS bispectrum for a cosmic-variance-limited experiment is about 5 for $l_{\rm max} = 1500$, which is smaller than the previous estimates [8, 9], but agrees well with the estimates based on the linear calculation [26–28].

We would like to thank J. Weller and D. Spergel for discussions. We would like to thank A. Lewis for pointing out that we should use the lensed C_l in Eq. (2) as well as the importance of the non-Gaussian contribution to the covariance matrix given in Eq. (19). This work is supported in part by NSF grant PHY-0758153.

[1] R. K. Sachs and A. M. Wolfe, Astrophys. J. **147**, 73 (1967).
[2] M. J. Rees and D. W. Sciama, Nature (London) **217**, 511 (1968).
[3] E. Komatsu *et al.* (WMAP Collaboration), Astrophys.J.Suppl. **192**, 18 (2011), arXiv:1001.4538 [astro-ph.CO].
[4] R. G. Crittenden and N. Turok, Phys.Rev.Lett. **76**, 575 (1996), arXiv:astro-ph/9510072 [astro-ph].
[5] A. Lewis and A. Challinor, Phys.Rept. **429**, 1 (2006), arXiv:astro-ph/0601594 [astro-ph].
[6] D. M. Goldberg and D. N. Spergel, Phys. Rev. D **59**, 103002 (1999), arXiv:astro-ph/9811251.
[7] L. Verde and D. N. Spergel, Phys. Rev. D **65**, 043007 (2002), arXiv:astro-ph/0108179.
[8] F. Giovi, C. Baccigalupi, and F. Perrotta, Phys. Rev. D **68**, 123002 (2003), arXiv:astro-ph/0308118; **71**, 103009 (2005), arXiv:astro-ph/0411702.
[9] A. Mangilli and L. Verde, Phys. Rev. D **80**, 123007 (2009), arXiv:0906.2317.
[10] E. Komatsu *et al.* (WMAP Collaboration), Astrophys.J.Suppl. **180**, 330 (2009), arXiv:0803.0547 [astro-ph].
[11] E. Komatsu and D. N. Spergel, Phys. Rev. D **63**, 063002 (2001), arXiv:astro-ph/0005036.
[12] A. Lewis, A. Challinor, and D. Hanson, JCAP **1103**, 018 (2011), arXiv:1101.2234 [astro-ph.CO].
[13] D. N. Spergel and D. M. Goldberg, Phys. Rev. D **59**, 103001 (1999), arXiv:astro-ph/9811252.
[14] F. Bernardeau, S. Colombi, E. Gaztañaga, and R. Scoccimarro, Phys.Rept. **367**, 1 (2002), arXiv:astro-ph/0112551.
[15] D. Jeong and E. Komatsu, Astrophys. J. **651**, 619 (2006), arXiv:astro-ph/0604075.
[16] A. J. Nishizawa, E. Komatsu, N. Yoshida, R. Takahashi, and N. Sugiyama, Astrophys. J. Lett. **676**, L93 (2008), arXiv:0711.1696.
[17] E. T. Vishniac, MNRAS **203**, 345 (1983); J. N. Fry, Astrophys. J. **279**, 499 (1984); M. H. Goroff, B. Grinstein, S.-J. Rey, and M. B. Wise, **311**, 6 (1986); Y. Suto and M. Sasaki, Physical Review Letters **66**, 264 (1991); N. Makino, M. Sasaki, and Y. Suto, Phys. Rev. D **46**, 585 (1992); B. Jain and E. Bertschinger, Astrophys. J. **431**, 495 (1994), arXiv:astro-ph/9311070.
[18] A. Cooray and R. Sheth, Phys.Rept. **372**, 1 (2002), arXiv:astro-ph/0206508.
[19] C. Ma, R. R. Caldwell, P. Bode, and L. Wang, Astrophys. J. Lett. **521**, L1 (1999), arXiv:astro-ph/9906174.
[20] R. E. Smith, J. A. Peacock, A. Jenkins, S. D. M. White, C. S. Frenk, F. R. Pearce, P. A. Thomas, G. Efstathiou, and H. M. P. Couchman, MNRAS **341**, 1311 (2003), arXiv:astro-ph/0207664.
[21] A. J. S. Hamilton, P. Kumar, E. Lu, and A. Matthews, Astrophys. J. Lett. **374**, L1 (1991).
[22] J. A. Peacock and S. J. Dodds, MNRAS **267**, 1020 (1994), arXiv:astro-ph/9311057.

[23] J. A. Peacock and S. J. Dodds, MNRAS **280**, L19 (1996), arXiv:astro-ph/9603031.
[24] D. J. Eisenstein and W. Hu, Astrophys.J. **496**, 605 (1998), arXiv:astro-ph/9709112 [astro-ph].
[25] W. H. Press, S. A. Teukolsky, W. T. Vetterling, and B. P. Flannery, (1992), cambridge University Press.
[26] K. M. Smith and M. Zaldarriaga, Mon.Not.Roy.Astron.Soc. **417**, 2 (2011), arXiv:astro-ph/0612571 [astro-ph].
[27] P. Serra and A. Cooray, Phys. Rev. D **77**, 107305 (2008), arXiv:0801.3276.
[28] D. Hanson, K. M. Smith, A. Challinor, and M. Liguori, Phys. Rev. D **80**, 083004 (2009), arXiv:0905.4732.
[29] P. Creminelli and M. Zaldarriaga, Journal of Cosmology and Astro-Particle Physics **10**, 6 (2004), arXiv:astro-ph/0407059.